HOSTED BY

ELSEVIER

Available online at www.sciencedirect.com

ScienceDirect

journal homepage: www.elsevier.com/locate/jtte

Original Research Paper

Application of semi-analytical finite element method coupled with infinite element for analysis of asphalt pavement structural response

Pengfei Liu[*], *Dawei Wang*, *Markus Oeser*

Faculty of Civil Engineering, RWTH Aachen University, Aachen D-52074, Germany

ARTICLE INFO

Article history:
Available online 20 January 2015

Keywords:
Asphalt pavement
Structural response
Semi-analytical finite element method
ABAQUS
Infinite element
Finite-infinite element coupling analysis

ABSTRACT

A specific computational program SAFEM was developed based on semi-analytical finite element (FE) method for analysis of asphalt pavement structural responses under static loads. The reliability and efficiency of this FE program was proved by comparison with the general commercial FE software ABAQUS. In order to further reduce the computational time without decrease of the accuracy, the infinite element was added to this program. The results of the finite-infinite element coupling analysis were compared with those of finite element analysis derived from the verified FE program. The study shows that finite-infinite element coupling analysis has higher reliability and efficiency.

1. Introduction

In the past decades, the finite element (FE) method has been developed rapidly and was increasingly used in many industrial fields as well as in the routine pavement design process. But there are several limitations in the conventional FE packages, such as the complexity of the program and hence the time-consuming user training process or over-simplifications of the modeling (Liu et al., 2014a). Therefore, it is necessary to find means that both improve the computational speed without increasing the resource requirement and keep the computational accuracy. One specified program SAFEM was developed based on the semi-analytical FE method to meet these requirements.

For a typical pavement structure problem as shown in Fig. 1, the geometry and material properties usually do not vary in the z-direction, but the boundary conditions, e.g. the load terms, exhibit a significant variation in that direction. Due to this characteristic, the pavement structure problem could not be simplified as a 2D plane strain case. An alternative method is to simplify the pavement structure as a 2D axisymmetric case, and the response under multiple loads can be obtained using superposition principle. However, the models based on the axisymmetric formulation cannot realistically model unidirectional loads, cracks or discontinuities within a pavement system and the ability to realistically model non-uniform contact pressures is also limited (Fritz, 2002). Zienkiewicz and Taylor (2005) proposed one method that assuming the displacements in the geometrical z-

* *Corresponding author*. Tel.: +49 241 8020389; fax: +49 241 80 22141.
E-mail address: liu@isac.rwth-aachen.de (P. Liu).
Peer review under responsibility of Periodical Offices of Chang'an University.
http://dx.doi.org/10.1016/j.jtte.2015.01.005

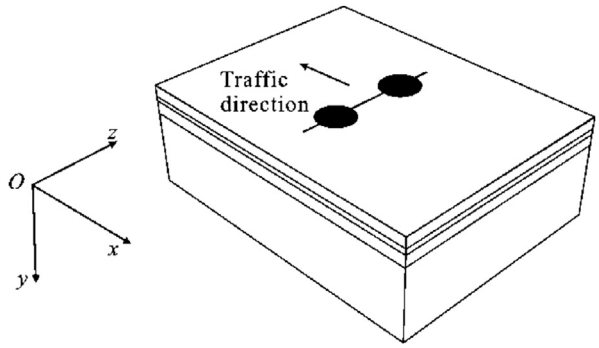

Fig. 1 – Pavement structure geometry and load mode (Liu et al., 2014a).

direction can be represented using Fourier series and exploiting its orthogonal properties, the problem of such a class can thus be simplified into a series of 2D solutions. This method is so called the semi-analytical FE method which has potential for overcoming the difficulties mentioned above.

The pavement length along the traffic direction and the thickness of sub-grade can be considered infinity. In order to minimize the influence of these boundaries, the FE-mesh must be sufficiently big in horizontal and vertical directions. This, however, means that a relatively large number of FE-elements are required to appropriately discretize the mesh. One of the methods that can keep the number of FE-elements reasonably low is the application of infinite elements at the infinite boundaries of the system in the FE method (Li et al., 2007b). This concept of the infinite element was firstly proposed by Ungless (1973), and then modified and further developed by many other researchers such as Beer and Meer (1981), Bettess (1977, 1980), Bettess and Zienkiewicz (1977), Zienkiewicz et al. (1983) and applied to a variety of problems (Hjelmstad et al., 1997; Li et al., 2007a; Wang and Brill, 2013). Currently, the infinite elements have been developed from one-dimensional (1D), unidirectional to 3D and multidirectional approaches. The concept of infinite elements can be generally divided into two categories: the mapping infinite element and decaying infinite element (Sallah and Buchanan, 1990). The features of the infinite elements can be concluded as follows (Jiang et al., 2009; Zhu and Bian, 2001):

- The mapping from finite field in the natural coordinate to infinite field in the global coordinate, e.g. when the natural coordinate ξ approaches 1 the corresponding global coordinate will trend towards infinity to fulfill the requirement that the computational field trends towards infinity.
- The decay of the displacement in the infinite field, e.g., when ξ approaches 1, the displacement tends towards 0 to fulfill the requirement of the boundary condition that the displacement at the infinity is 0.

In the following sections, the mathematical basis of the SAFEM and the 2D mapping infinite element will be presented at first, followed by a verification of the SAFEM by comparison with ABAQUS as well as a verification of the finite-infinite element coupling analysis in the SAFEM program. Finally, a brief summary and conclusions are provided at the end of this paper.

2. Description of semi-analytical finite element method

The first step in the FE formulation of SAFEM is to express the element coordinates and element displacements in the form of interpolation functions using the natural coordinate system of the element.

By using the SAFEM, the general form of the shape functions can be written as a Fourier series in which z ranges between 0 and a (Fritz, 2002; Hu et al., 2008; Liu et al., 2013, 2014a, 2014b; Zienkiewicz and Taylor, 2005), as shown in Fig. 2.

$$u = \sum_{k=1}^{6} N_k(x,y,z)u_k = \sum_{l=1}^{L}\sum_{k=1}^{6}\left\{\left[\overline{N_k}(x,y)\cos\frac{l\pi z}{a}\right] + \left[\overline{\overline{N_k}}(x,y)\sin\frac{l\pi z}{a}\right]\right\}u_k^l \quad (1)$$

where l identifies the term of the Fourier series, L is the total number of Fourier terms considered, $\overline{N_k}$ and $\overline{\overline{N_k}}$ are the shape functions of the element at node k.

The loading function defining the variation of load along the z-direction is given by Zienkiewicz and Taylor (2005).

$$f = \sum_{l=1}^{L}\left\{\left[\overline{p}(x,y)\cos\frac{l\pi z}{a}\right] + \left[\overline{\overline{p}}(x,y)\sin\frac{l\pi z}{a}\right]\right\} \quad (2)$$

where $\overline{p}(x,y)$ and $\overline{\overline{p}}(x,y)$ represent the pavement load.

The pavement is assumed to be supported on both side faces ($z = 0$ and $z = a$) in a manner preventing all displacements in the xy plane but permitting "unrestricted" motion in the z-direction. The Fourier series expansion should meet this requirement of the boundary condition. The displacement functions with three components u, v and w can be written as follow

$$U = \begin{Bmatrix} u \\ v \\ w \end{Bmatrix} = \sum_{l=1}^{L}\sum_{k=1}^{6} N_k \begin{bmatrix} \sin\frac{l\pi z}{a} & 0 & 0 \\ 0 & \sin\frac{l\pi z}{a} & 0 \\ 0 & 0 & \cos\frac{l\pi z}{a} \end{bmatrix} \begin{Bmatrix} u_k^l \\ v_k^l \\ w_k^l \end{Bmatrix} = \sum_{l=1}^{L} N^l \cdot U^l \quad (3)$$

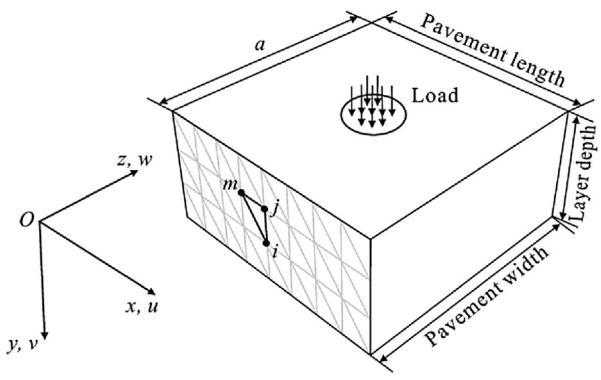

Fig. 2 – Schematic representation of a SAFEM situation (Liu et al., 2014a).

where u_k^l, v_k^l and w_k^l are the displacements of the node at the Fourier term k in x-, y- and z-directions, respectively.

Similarly, the loading function for the pavement analysis can be formulated as follows (Fritz, 2002)

$$f = \sum_{l=1}^{L} p(x,y)\sin\frac{l\pi z}{a} = \sum_{l=1}^{L}\{p\}^l \tag{4}$$

$$p(x,y) = \sum_{t=1}^{n}\left(\frac{2P_t}{l\pi}\right)\left(\cos\frac{l\pi}{a}Z_{t1} - \cos\frac{l\pi}{a}Z_{t2}\right) \tag{5}$$

where P_t is the tire load pressure, Z_{t1} is the z coordinate where the tire load area starts, Z_{t2} is the z coordinate where the tire load area ends.

By using the principle of minimum potential energy, a typical sub-matrix of the element stiffness matrix $(K^{lm})^e$ is (Hu et al., 2008)

$$\left(K^{lm}\right)^e = \iiint_{vol}\left(B^l\right)^T D B^m \mathrm{d}x\mathrm{d}y\mathrm{d}z \tag{6}$$

One detail worth to be mentioned is the decomposition of the strain-displacement matrix B_k^l as follow

$$\begin{aligned} B_k^l &= \begin{bmatrix} \frac{\partial N_k}{\partial x}\sin\frac{l\pi z}{a} & 0 & 0 \\ 0 & \frac{\partial N_k}{\partial y}\sin\frac{l\pi z}{a} & 0 \\ 0 & 0 & -\frac{l\pi}{a}N_k\sin\frac{l\pi z}{a} \\ \frac{\partial N_k}{\partial y}\sin\frac{l\pi z}{a} & \frac{\partial N_k}{\partial x}\sin\frac{l\pi z}{a} & 0 \\ 0 & \frac{l\pi}{a}N_k\cos\frac{l\pi z}{a} & \frac{\partial N_k}{\partial y}\cos\frac{l\pi z}{a} \\ \frac{l\pi}{a}N_k\cos\frac{l\pi z}{a} & 0 & \frac{\partial N_k}{\partial x}\cos\frac{l\pi z}{a} \end{bmatrix} \\ &= \overline{B}_k^l\sin\frac{l\pi z}{a} + \overline{\overline{B}}_k^l\cos\frac{l\pi z}{a} \end{aligned} \tag{7}$$

The B_k^l in Eq. (7) is splitted into two matrices of which each only includes one type of trigonometric terms.

From Eqs. (6) and (7), the stiffness matrix of one element includes (Zienkiewicz and Taylor, 2005)

$$\begin{aligned} &I_1 = \int_0^a \frac{\sin l\pi z}{a}\cdot\frac{\cos m\pi z}{a}\mathrm{d}z, \quad I_2 = \int_0^a \frac{\sin l\pi z}{a}\cdot\frac{\sin m\pi z}{a}\mathrm{d}z, \\ &I_3 = \int_0^a \frac{\cos l\pi z}{a}\cdot\frac{\cos m\pi z}{a}\mathrm{d}z \end{aligned} \tag{8}$$

The integrals exhibit orthogonal properties which ensure that

$$I_2 = I_3 = \begin{cases} \frac{1}{2}a & for\ l = m \\ 0 & for\ l \neq m \end{cases} \tag{9}$$

Only when l and m are both odd or even numbers, the first integral I_1 is zero. But due to the special structure of the B^l matrix, all terms that include I_1 vanish (becoming 0). This means that the matrix $(K^{lm})^e$ becomes a diagonal one. In other words, the non-zero values are only located in the diagonal area where $l = m$. Thus, the stiffness matrix can be reduced to (Zienkiewicz and Taylor, 2005)

$$\left(K_{gk}^{ll}\right)^e = \frac{1}{2}a\iint_{area}\left[\left(\overline{B}_g^l\right)^T D\overline{B}_k^l + \left(\overline{\overline{B}}_g^l\right)^T D\overline{\overline{B}}_k^l\right]\mathrm{d}x\mathrm{d}y \quad l = 1, 2\cdots \tag{10}$$

where g and k represent the nodes of the element, respectively, *area* is the area of the element.

A typical term for the force vector becomes

$$\left(F^l\right)^e = \iiint_{vol}\left(N^l\right)^T\{p\}^l\mathrm{d}x\mathrm{d}y\mathrm{d}z \tag{11}$$

The final assembled equations have the following form

$$\begin{bmatrix} K^{11} & & & \\ & K^{22} & & \\ & & \ddots & \\ & & & K^{LL} \end{bmatrix}\begin{Bmatrix} U^1 \\ U^2 \\ \vdots \\ U^L \end{Bmatrix} + \begin{Bmatrix} F^1 \\ F^2 \\ \vdots \\ F^L \end{Bmatrix} = 0 \tag{12}$$

Eq. (12) shows that the large system of equations splits up into L separate problems.

$$K^{ll}U^l + F^l = 0 \tag{13}$$

According to Eq. (13), the Fourier expansion of the loading factors involves only one term for a particular harmonic, so only one set of simultaneous equations needs to be solved. This solution is just like a 2D plane problem. The sub-displacement vector calculated from each term of Fourier series only needs to be assembled to a global vector.

3. Description of 2D mapping infinite element method

Due to the 2D mesh of the finite elements used in the SAFEM, only 2D mapping infinite elements which were applied in this program are introduced in this section. The 2D mapping infinite elements can be divided into two types which are unidirectional and bidirectional ones.

3.1. *Formulation of 2D mapping infinite elements*

Fig. 3(a) shows the 2D unidirectional infinite element which extends to infinity in y-direction. The nodes 1, 2 and 3 are at the interface which can be coupled with finite elements and the nodes 4 and 5 are in the middle of the infinite element. Fig. 3(b) shows the bidirectional infinite element, in which the node 1 can be coupled with a finite element and nodes 2 and 3 are in the "middle" of the infinite element. Through mapping the infinite reference element is transferred from the global coordinate to a parent element in a finite region, i.e. the element in natural coordinate with $-1 \le \xi \le 1$ and $-1 \le \eta \le 1$.

The transformation equations, or the mapping infinite element, between the global and natural coordinates are (Zhao, 2012; Zhou et al., 2004)

$$\begin{aligned} &x = \sum_{i=1}^{n} M_i x_i, \\ &y = \sum_{i=1}^{n} M_i y_i \quad \begin{cases} n = 5 & for\ unidirectional\ infinite\ element \\ n = 3 & for\ bidirectional\ infinite\ element \end{cases} \end{aligned} \tag{14}$$

where the node-wise mapping functions $\sum M_i = 1$, as shown in Table 1.

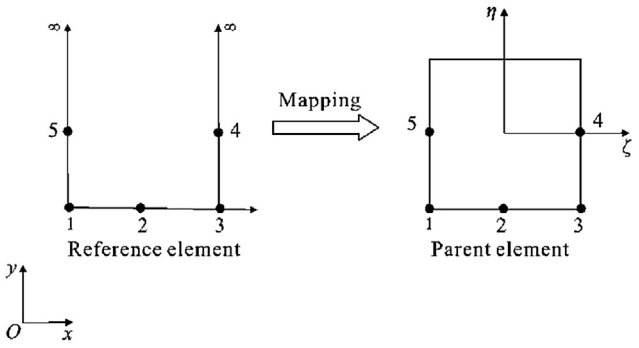

(a) 2D unidirectional mapping infinite element

(b) 2D bidirectional mapping infinite element

Fig. 3 – 2D mapping infinite elements.

The displacement of any point in the parent element can be expressed as follows (Zhao, 2012; Zhou et al., 2004)

$$u=\sum_{i=1}^{n}N_i u_i,\qquad v=\sum_{i=1}^{n}N_i v_i\quad\begin{cases}n=5 & \textit{for unidirectional infinite element}\\ n=3 & \textit{for bidirectional infinite element}\end{cases}\tag{15}$$

where shape function N_i can be seen in Table 1.

If only the finite elements are used, the calculation of stiffness matrix only involves the shape function. When the infinite elements are applied, the calculation of their displacement still uses the shape function, while the coordinate transformation of the infinite elements must use the mapping function.

3.2. *Finite-infinite element coupling method*

When analyzing a problem with an infinite domain, the infinite elements can be combined with the finite element method, i.e. the near field is analyzed by finite elements and the far field is simulated by infinite elements. As a result, the problem with continuous infinite degrees of freedom can be converted into one with discretized finite degrees of freedom. The unknown displacement at any node in the computational domain can be computed from the equilibrium equations, which are derived from the equilibrium conditions and the consistency of displacements at the interface between finite and infinite elements. The general procedure of the finite-infinite element coupling method is illustrated as follows (Zhao, 2012).

- The equations are built up in the near and far field, respectively.

$$\begin{cases}L_1(\{C^1\},\{F^1\})=0\\ L_2(\{C^2\},\{F^2\})=0\end{cases}\tag{16}$$

where {C} is unknown variable, {F} is the interaction force at the interface, 1 and 2 represent the finite element and infinite element fields, respectively.

- Derivation of the displacement expression at the interface

$$\begin{cases}\{U^1\}=f_1(\{C^1\},\{F^1\})\\ \{U^2\}=f_2(\{C^2\},\{F^2\})\end{cases}\tag{17}$$

- Establishment of the continuous equations at the interface

$$\begin{cases}\{U^1\}=\{U^2\}\\ \{F^1\}+\{F^2\}=\{0\}\end{cases}\tag{18}$$

The three equations are combined and solved to derive the $\{C^1\}$ and $\{C^2\}$. And then the $\{U^1\}$, $\{U^2\}$ and other variables such as the strain and stress can be calculated.

In order to simulate the infinite domain of the asphalt pavement, the infinite element was added to SAFEM first. The theoretical derivations and computational procedures of the stiffness matrix in finite element method and finite-infinite element coupling method are relatively similar, which is convenient for the application of the infinite elements. The global stiffness of the nodes at the interface can be calculated as the sum of the nodal stiffness of the finite and infinite element (Jiang et al., 2009).

Table 1 – Formula of mapping and shape function for the 2D mapping infinite element.

Infinite element type	Mapping function	Shape function
Unidirectional	$M_1=(1-\xi)(-1-\xi-\eta)/1-\eta$	$N_1=1/4(1-\xi)(1-\eta)(-1-\xi-\eta)$
	$M_2=2(1-\xi^2)/1-\eta$	$N_2=½(1-\xi^2)(1-\eta)$
	$M_3=(1+\xi)(-1+\xi-\eta)/1-\eta$	$N_3=1/4(1+\xi)(1-\eta)(-1+\xi-\eta)$
	$M_4=(1+\xi)(1+\eta)/2(1-\eta)$	$N_4=½(1+\xi)(1-\eta^2)$
	$M_5=(1-\xi)(1+\eta)/2(1-\eta)$	$N_5=½(1-\xi)(1-\eta^2)$
Bidirectional	$M_1=\xi\eta+3(-1-\xi-\eta)/(1-\xi)(1-\eta)$	$N_1=1/4(1-\xi)(1-\eta)(-1-\xi-\eta)$
	$M_2=2(1+\xi)/(1-\xi)(1-\eta)$	$N_2=½(1-\xi^2)(1-\eta)$
	$M_3=2(1+\eta)/(1-\xi)(1-\eta)$	$N_3=½(1-\xi)(1-\eta^2)$

$$\begin{bmatrix} \cdots & \cdots & \cdots \\ \cdots & k_{ij} & \cdots \\ \cdots & \cdots & \cdots \end{bmatrix} = \begin{bmatrix} \cdots & \cdots & \cdots \\ \cdots & k_{ij}^{1} & \cdots \\ \cdots & \cdots & \cdots \end{bmatrix} + \begin{bmatrix} \cdots & \cdots & \cdots \\ \cdots & k_{ij}^{2} & \cdots \\ \cdots & \cdots & \cdots \end{bmatrix} \quad (19)$$

where k_{ij} is the nodal stiffness in the global stiffness matrix, k_{ij}^{1} and k_{ij}^{2} are the stiffness of node in the finite and infinite elements, respectively, i and j are the address indicators of the node.

4. Verification of SAFEM by comparison with ABAQUS

The accuracy of the SAFEM only with finite elements was verified by comparison with the results derived from the general commercial FE-program ABAQUS (ABAQUS, 2011). The parameters and boundary conditions in the modeling of these two programs were selected as consistent as possible to ensure a high comparability of the models.

4.1. *Definition of the models*

The responses from both models were evaluated using the pavement type in Table 2, which is widely used in Germany according to the guidelines RStO 01 (FGSV, 2002) and RDO Asphalt 09 (FGSV, 2009). The thicknesses of all layers excepting the sub-grade were derived from RStO 01 (FGSV, 2002). The thickness of the sub-grade was defined as 2000 mm. Setting such a large value was aimed to minimize the influence of the boundary condition on the results. Besides, the length and width of all layers were set to 6000 mm for the same reason. The pavement surface temperatures of −12.5 °C (winter) and 27.5 °C (summer) were assumed, and then the associated material properties in the superstructure were determined according to RDO Asphalt 09 (FGSV, 2009), as listed in Fig. 4 and Table 2.

The mesh generator of SAFEM was used to create a 2D mesh in the xy plane consisting of 6-node triangular elements, as shown in Fig. 5(a). While the model in ABAQUS was three-dimensional, so the type of 3D 10-node quadratic tetrahedron element was applied in order to make the mesh geometry as close as possible to that in SAFEM. The mesh in ABAQUS is illustrated in Fig. 5(b). Due to the different dimensions of both models, the mesh algorithms are different, but the element size increases gradually from the loading area in both models.

Table 2 – Geometrical data and material properties of the pavement.

Layer	μ	Winter	Summer
		E (MPa)	E (MPa)
Surface course	0.35	22,690	2902
Binder course	0.35	27,283	6817
Asphalt base curse	0.35	17,853	4903
Road base course	0.25	10,000	10,000
Sub-base	0.50	100	100
Sub-grade	0.50	45	45

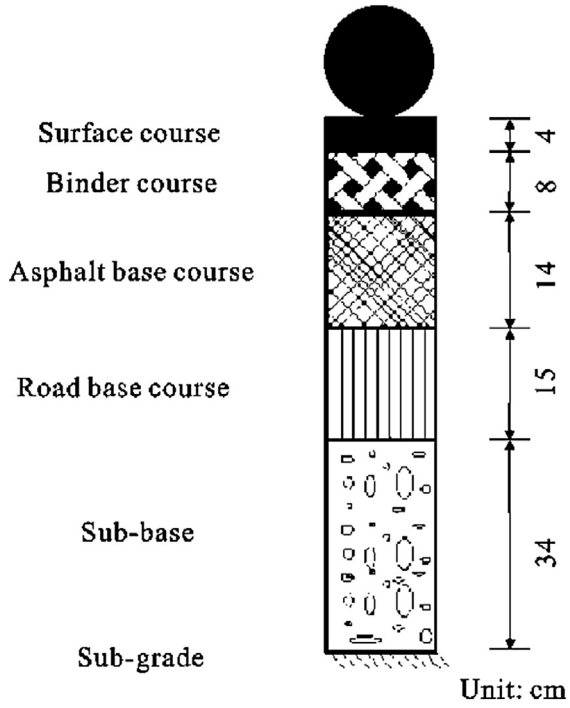

Fig. 4 – Structure of the pavement.

The number of elements in SAFEM and ABAQUS are 2272 and 49,671, respectively.

According to RDO Asphalt 09 (FGSV, 2009), the load adopted in SAFEM and ABAQUS was 49 kN circular load with the radius of 150 mm, so the uniformly distributed contact stress was 0.7 MPa. The loading area was located at the center of the pavement illustrated in Fig. 2.

The bottom nodes of the mesh representing the sub-grade in both models were fixed in all directions. According to the theory of SAFEM, the displacements on both edges ($z = 0$ and $z = a$) are restricted to zero in the x- and y-directions. The same boundary conditions were also used for the ABAQUS model. The three asphalt layers are totally bound and the two contact layers among the asphalt base course, road base course, sub-base and sub-grade are defined as being partially bound, which means the nodes at the interface between the different layers always have the same displacements in the vertical direction but may have different displacements in the horizontal direction.

4.2. *Comparison of the results between ABAQUS and SAFEM*

The computed results from both models are compared in Moiré pattern, as shown in Fig. 6. The cross-section is the inner surface with $x = 3000$ mm. It can be seen that the distribution of the stresses and the deformation shapes from both FE programs are consistent.

The computational stresses shown in Figs. 7–10 are derived from four series of response points offset from the

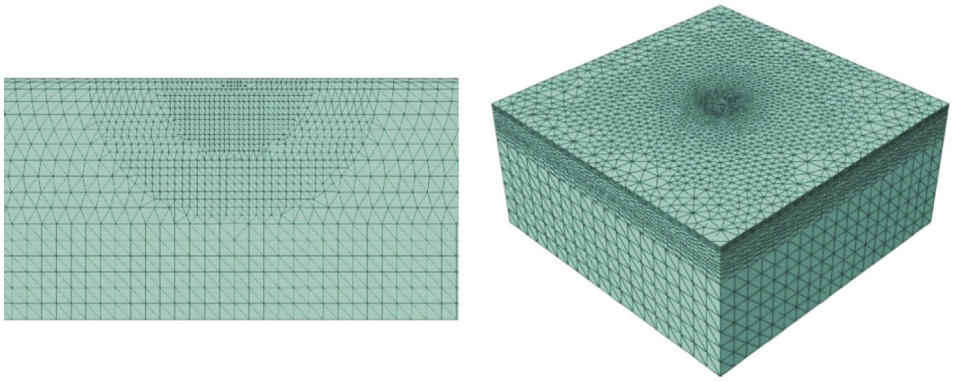

Fig. 5 – Mesh automatically generated from two FE-programs.

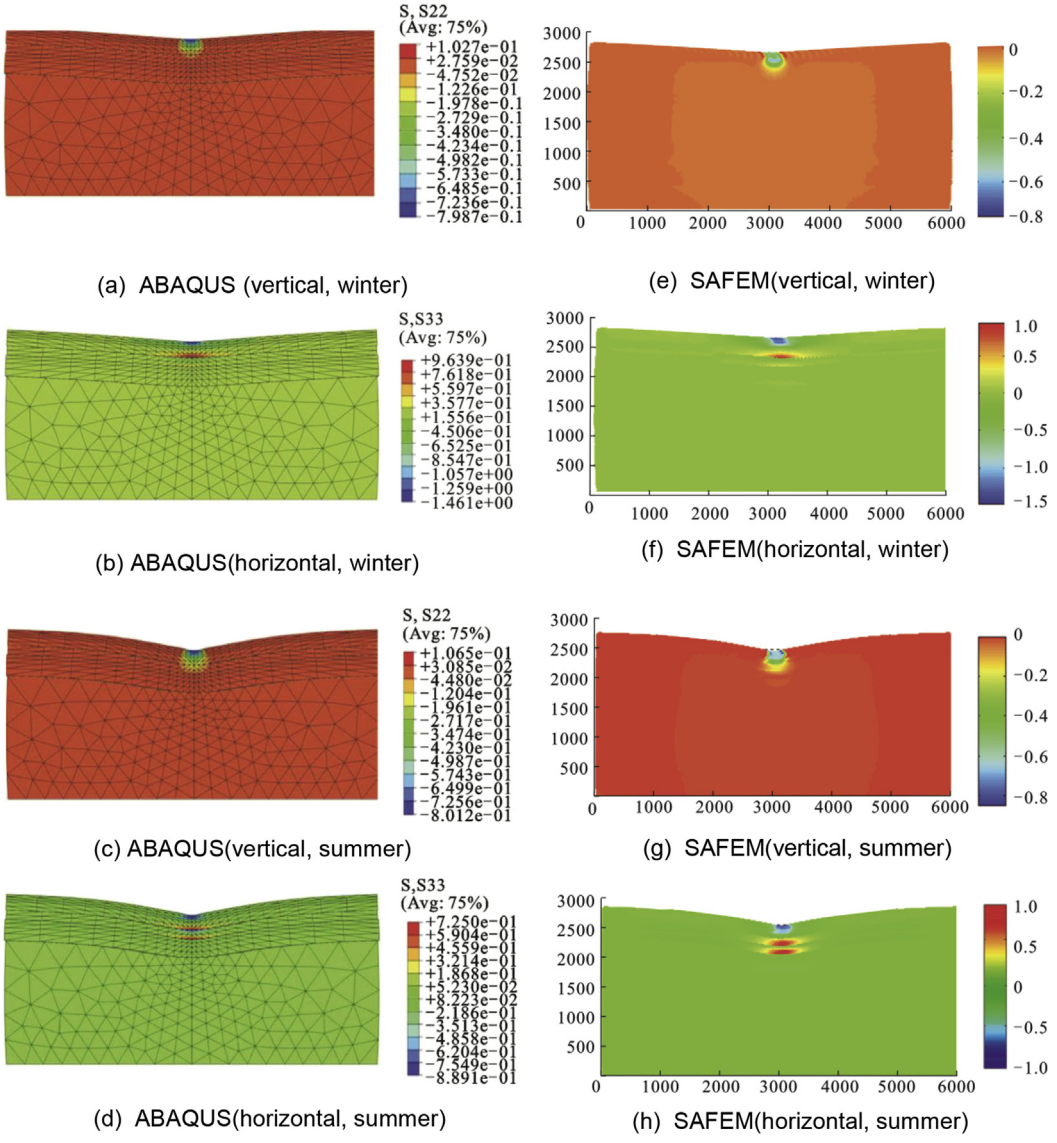

Fig. 6 – Computational stress and deformation from ABAQUS and SAFEM.

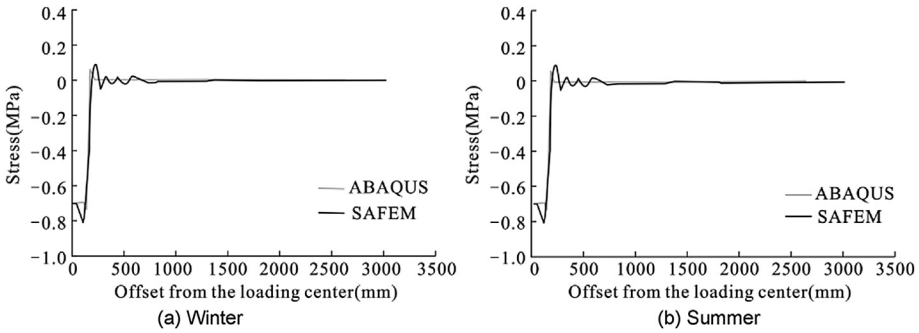

Fig. 7 – Comparison of vertical stress on the top of asphalt surface course derived from ABAQUS and SAFEM.

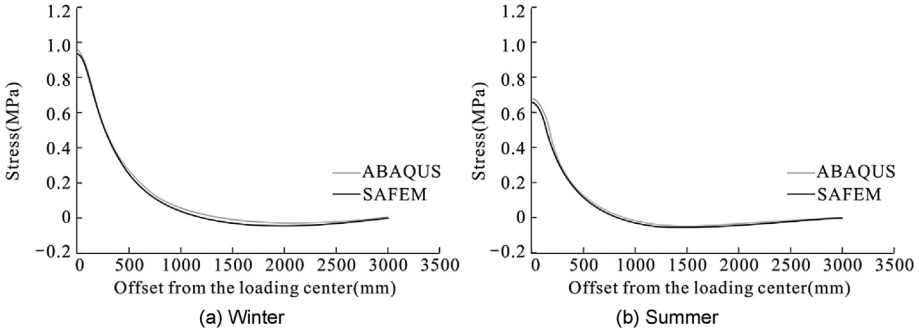

Fig. 8 – Comparison of horizontal stress on the bottom of asphalt base course derived from ABAQUS and SAFEM.

loading center to the boundary (*x* coordinate from 3000 to 6000 mm in SAFEM of Fig. 6).

In Table 3, the vertical and horizontal stresses at four critical points directly below the loading center, where maximum compressive or tensile stresses may occur, are considered. From Figs. 7–10, and Table 3, it can be stated that the results from both programs have a high correlation except for a slightly larger difference in the vertical stresses on the top of the sub-base. The computation time of the SAFEM is much shorter than that of the ABAQUS. Both FE analyses were run on a computer with an Intel Core Duo 3.4 GHz, 32 GB RAM. On average, the computational time required by the ABAQUS 3D model is about 220 s, whereas the SAFEM model requires 11 s. With code optimization, the computational time of the SAFEM may be further reduced.

5. Verification of finite-infinite element coupling analysis in SAFEM

5.1. *Definition of the models*

The reliability and efficiency of the finite-infinite element coupling analysis in the SAFEM were studied by comparison of the results with those from the SAFEM which have been proved to be reliable in the section above. The asphalt pavement structural responses from both analyses were evaluated using the same pavement type with the material properties shown in Table 2 (winter case).

The thicknesses of all layers excepting the sub-grade were reference to Table 2. The thickness of the sub-grade was

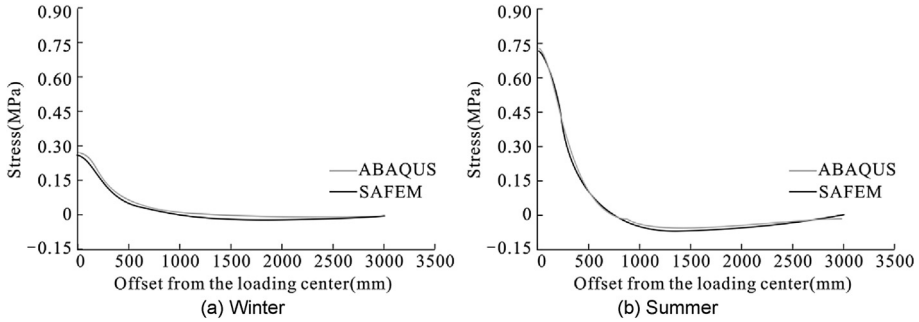

Fig. 9 – Comparison of horizontal stress on the bottom of road base course derived from ABAQUS and SAFEM.

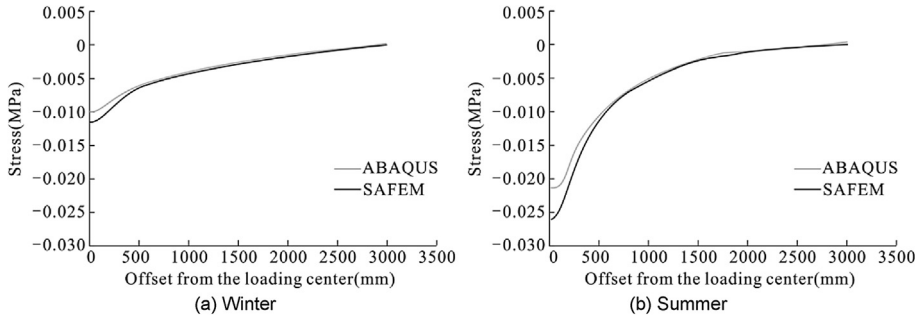

Fig. 10 – Comparison of vertical stress on the top of sub-grade derived from ABAQUS and SAFEM.

Table 3 – Comparison between ABAQUS and SAFEM regarding the determined stresses (MPa) at critical points.

Points	Winter			Summer		
	SAFEM	ABAQUS	Difference	SAFEM	ABAQUS	Difference
1	−0.704	−0.704	0.000 (0%)	−0.698	−0.702	0.004 (0.57%)
2	0.938	0.959	−0.021 (2.19%)	0.663	0.675	−0.012 (1.78%)
3	0.262	0.269	−0.007 (2.60%)	0.715	0.725	−0.010 (1.38%)
4	−0.010	−0.009	−0.001 (11.1%)	−0.027	−0.022	−0.005 (22.7%)

defined from 100 to 9000 mm. Setting such a series of values is aimed to investigate the influence of the sub-grade thickness on the results. The length of each layer along traffic direction was set from 3500 to 30,000 mm for the similar reason. The width of the pavement was still set to 6000 mm.

The mesh generator of SAFEM was used to create a 2D mesh consisting of 6-node triangular finite elements for the finite element analysis (Persson and Strang, 2004) as shown in Fig. 11(a). When coupled with infinite elements, the 5-node unidirectional or 3-node bidirectional mapping infinite elements were created outside the finite element domain, as shown in Fig. 11(b). If the geometrical parameters are the same, the numbers of the finite elements are also the same in both analyses, but the finite-infinite element coupling analysis has several additional infinite elements.

The load and the condition of interlayer connection were defined as the same with that used in the Section 4.1. The bottom nodes of the mesh representing the sub-grade in the finite element analysis were fixed in all directions, but in the finite-infinite element coupling analysis this boundary condition was not necessary.

5.2. *Comparison of the results between finite element analysis and finite-infinite element coupling analysis*

Four response points from the same critical points in Section 4.1 were selected to compare the results of both analyses.

If the pavement length is kept as 30,000 mm which is considered to be large enough and hence does not influence the computational results, a series of results are derived with increasing the sub-grade thickness of the pavement, as shown in Fig. 12.

When the results from both analyses come to convergence, the absolute values of the results from the finite-infinite element coupling analysis are a little larger than those from the finite element analysis. All the relative errors of the four response points (take the results of the finite element analysis as reference) are below 1.3%, which proves the reliability of the finite-infinite element coupling analysis in the SAFEM. Furthermore, in the prediction of the pavement remaining service life, the slightly larger stress values will make the prediction result "safer", which even has a certain positive significance.

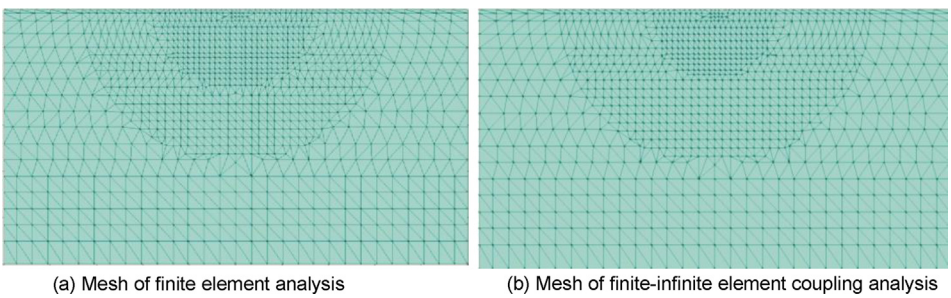

Fig. 11 – Mesh generated by SAFEM.

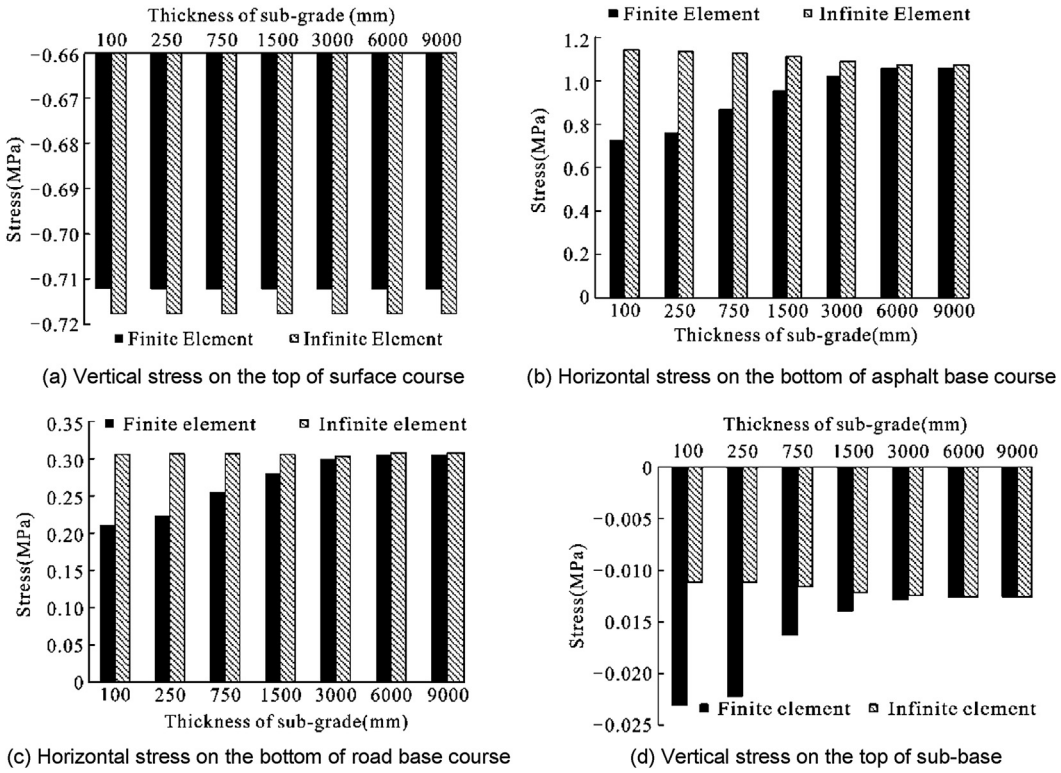

Fig. 12 – Comparison of the results when the pavement length is kept constant.

The vertical stress on the top of the surface course does not vary significantly, which means the thickness of the sub-grade almost does not influence the stress on the pavement surface. However, with increasing depth of the response points in the pavement, the stresses vary more significantly, especially on the top of the sub-base, i.e. the influence of the sub-grade thickness becomes more and more significant on stress state of deeper location in the pavement.

Comparing the results between the two analyses, the influence of the sub-grade thickness on the results from finite element analysis is much more significant. If its own convergence value is taken as reference, all the relative errors of the four response points reach the level below 3.5% in the finite element analysis when the thickness of sub-grade comes to be 3000 mm, while the thickness in finite-infinite element coupling analysis only needs to be 1500 mm.

Similarly, when the thickness of sub-grade is kept as 7500 mm which does not influence the computational results, a series of results from both analyses are derived with increasing the pavement length, as shown in Fig. 13.

Except for the stress on the top of the surface course, the stresses at the other response points vary similarly significantly, which means the influence of the pavement length on the stress is great regardless of the depth of the response points. The convergence rate of the finite-infinite element coupling analysis is still obviously higher than that of the finite element analysis, i.e. when the pavement length reaches 3500 mm in the finite-infinite element coupling analysis the relative errors become below 3%, while the length in finite element analysis needs to be 5000 mm to reach this level.

In order to compare the computational accuracy and time between the two analyses, two cases were studied as shown in Table 4. The two analyses were run on a computer with an Intel Core Duo 3.4 GHz, 32 GB RAM. If the minimum values of sub-grade thickness and pavement length (Case 1) is applied in previous investigation in both analyses, the accuracy of the finite-infinite element coupling analysis still keeps a relatively high level, but that of the finite element analysis decreases extremely. Although the finite-infinite element coupling analysis has additional nodes of the infinite elements, it does not need to determine constrain condition on the boundary, as a result the computational time (9 s) is even less than that of the finite element analysis (11 s). In order to keep the relatively high accuracy level in both analyses, the geometrical parameters were increased to different levels as shown in Case 2. In this case the computational time of the finite-infinite element coupling analysis (14 s) is only 70% of that of the finite element analysis (20 s), which reveals the higher computational efficiency of the finite-infinite element analysis.

6. Conclusions

This paper proposes to use the SAFEM for predicting the asphalt pavement structural responses under static loads. A computer program was developed based on MATLAB in which the SAFEM was applied. The accuracy of the program is

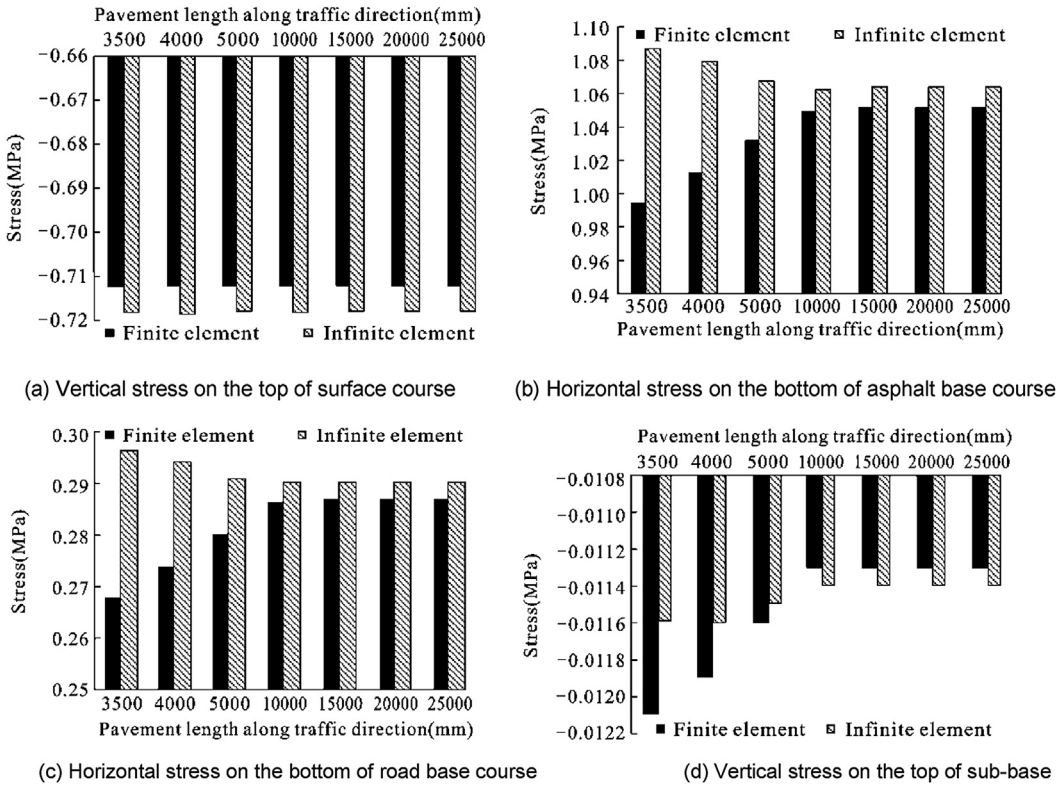

Fig. 13 – Comparison of the results when the thickness of sub-grade is constant.

Table 4 – Comparison of the relative errors and computational times from both analyses.

Item		Case 1		Case 2	
		Finite	Infinite	Finite	Infinite
Thickness of sub-grade (mm)		100	100	3000	1500
Pavement length (mm)		3500	3500	5000	3500
Relative error (%)	Top of the asphalt surface course	−0.04	0.03	0.01	0.00
	Bottom of the asphalt base course	−25.04	4.49	−3.58	3.54
	Bottom of the road base course	−24.21	1.89	−3.48	3.44
	Top of the sub-base	107.08	−12.28	5.31	−1.75
Computational time(s)		11	9	20	14

verified by a comparison with ABAQUS. Pavement responses to a static load predicted by SAFEM and ABAQUS are in very good agreement. Furthermore, the computational time of the SAFEM is much shorter than that of the ABAQUS.

In order to further reduce the computational time, the infinite elements are coupled with the finite elements in the SAFEM. The investigation shows that the results of the finite-infinite element coupling analysis are reliable and its convergence rate is much higher than that of the finite element analysis in the SAFEM. As a result, the scale of the pavement model at the infinite domain can be controlled in a suitable level and the computational time can be reduced without decreasing its accuracy.

For further investigation, the SAFEM allows the application of dynamic analysis and various material properties, such as viscoelasticity for asphalt and nonlinear elasticity for sub-base of the pavement. Furthermore, the regulation of the minimum amount of the finite elements required to be used in the finite-infinite element coupling analysis should be determined by the theoretical research and large numbers of case studies.

Acknowledgments

The work is part of a research project represented by German Federal Highway Research Institute (BASt), financed by the Federal Minister of Transport and Digital Infrastructure (BMVI), and conducted under FE 04.0259/2012/NGB.

REFERENCES

ABAQUS, 2011. ABAQUS Analysis User's Manual. Dassault Systemes Simulia Corp., Providence RI.

Beer, G., Meer, J.L., 1981. Infinite domain element. International Journal for Numerical Methods in Engineering 17, 43–52.
Bettess, P., 1977. Infinite elements. International Journal for Numerical Methods in Engineering 11, 53–64.
Bettess, P., 1980. More on infinite elements. International Journal for Numerical Methods in Engineering 15, 1613–1626.
Bettess, P., Zienkiewicz, O.C., 1977. Diffraction and refraction of surface waves using finite and infinite elements. International Journal for Numerical Methods in Engineering 11, 1271–1290.
FGSV, 2002. Guidelines for the Standardization of the Upper Structure of Traffic Areas (RStO 01), 2001 ed. FGSV Publisher, Research Society for Road and Transportation, Cologne.
FGSV, 2009. Guidelines for the Computational Dimension of the Upper Structure of Road with Asphalt Surface Course (RDO Asphalt 09), 2009 ed. FGSV Publisher, Research Society for Road and Transportation, Cologne.
Fritz, J.J., 2002. Flexible pavement response evaluation using the semi-analytical finite element method. International Journal of Materials and Pavement Design 3 (2), 211–225.
Hjelmstad, K.D., Zuo, Q., Kim, J., 1997. Elastic pavement analysis using infinite elements. Transportation Research Board 1568, 72–76.
Hu, S., Hu, X., Zhou, F., 2008. Using semi-analytical finite element method to evaluate stress intensity factors in pavement structure. In: Proceedings of the 6th RILEM International Conference on Cracking in Pavement, Chicago, 2008.
Jiang, Y., Chen, D., Yao, Y., 2009. Application of finite element and infinite element method to stress analysis of gravity dam. Engineering Journal of Wuhan University 42, 322–325.
Li, L., Kunimatsu, S., Wang, A., 2007a. Application of the generalized infinite element method to unbounded elasto-static problems. In: Proceedings of the ICCM2007, Hiroshima, 2007.
Li, L., Kunimatsu, S., Wang, A., 2007b. The infinite element method and its application. Advances in Mechanics 37 (2), 161–174.
Liu, P., Chen, X., Oeser, M., et al., 2014a. Application of semi-analytical finite element method in analysis of asphalt pavement structural response. In: Proceedings of 12th International Conference on Asphalt Pavements, Raleigh, 2014.
Liu, P., Wang, D., Oeser, M., 2013. Leistungsfähige semi-analytische methoden zur berechnung von Asphaltbefestigungen. In: 3rd Dresdner Asphalttage, Dresden, 2013.
Liu, P., Wang, D., Oeser, M., et al., 2014b. Einsatz der semi-analytischen finite-elemente-methode zur beanspruchungszustände von asphaltbefestigungen. Bauingenieur 89 (7/8), 333–339.
Persson, P.O., Strang, G., 2004. A simple mesh generator in MATLAB. Society for Industrial and Applied Mathematics 46 (2), 329–345.
Sallah, M., Buchanan, G.R., 1990. Some simplified methods for infinite elements. Computational Mechanics 6, 167–172.
Ungless, R.F., 1973. An Infinite Finite Element. Master thesis. University of British Columbia, Vancouver.
Wang, Q., Brill, D.R., 2013. Improvements in the application of infinite elements to the NIKE3D program for airport pavement response analysis. International Journal of Pavement Engineering 14 (5), 429–439.
Zhao, B., 2012. Dynamic Analysis of Semi-infinite Soil Based on Finite-element and Infinite-element Coupling Method. Master thesis. Beijing Jiaotong University, Beijing.
Zhou, S., Hu, X., Wang, J., 2004. The application of infinite element in numerical analysis of geotechnical engineering. Journal of Chongqing Jiaotong University 23, 61–64.
Zhu, J., Bian, C., 2001. The analysis method and its application in excavation which couples the finite element and infinite element. Ground Improvement 12 (3), 17–22.
Zienkiewicz, O.C., Emson, C., Bettess, P., 1983. A novel boundary infinite element. International Journal for Numerical Methods in Engineering 19, 393–404.
Zienkiewicz, O.C., Taylor, R.L., 2005. The Finite Element Method for Solid and Structural Mechanics, sixth ed. Elsevier Butterworth-Heinemann, Oxford.